AN ANALYSIS OF THE TIME SCALES OF VARIABILITY IN CENTURIES-LONG ENSO-SENSITIVE RECORDS IN THE LAST 1000 YEARS

HENRY F. DIAZ and ROGER S. PULWARTY

NOAA/ERL/CDC, 325 Broadway, Boulder, CO 80303, U.S.A., Cooperative Institute for Research in Environmental Sciences, and Department of Geography, University of Colorado, Boulder, CO 80309, U.S.A.

Abstract. We document the characteristic time scales of variability for seven climate indices whose time-dependent behavior is sensitive to some aspect of the El Niño/Southern Oscillation (ENSO). The ENSO sensitivity arises from the location of these long-term records on the periphery of the Indian and Pacific Oceans. Three of the indices are derived principally from historical sources, three others consist of tree-ring reconstructions (one of summer temperature, and the other two of winter rainfall), and one is an annual record of oxygen isotopic composition for a high-elevation glacier in Peru. Five of the seven indices sample at least portions of the Medieval Warm Period (~ A.D. 950 to 1250).

Time series spectral analysis was used to identify the major time scales of variability among the different indices. We focus on two principal time scales: a high frequency band (~ 2–10 yr), which comprises most of the variability found in the modern record of ENSO activity, and a low frequency band to highlight variations on decadal to century time scales ($11 < P < 150$ yr). This last spectral band contains variability on time scales that are of general interest with respect to possible changes in large-scale air-sea exchanges. A technique called evolutive spectral analysis (ESA) is used to ascertain how stable each spectral peak is in time. Coherence and phase spectra are also calculated among the different indices over each full common period, and following a 91-yr window through time to examine whether the relationships change.

In general, spectral power on time scales of ~ 2–6 yr is statistically significant and persists throughout most of the time intervals sampled by the different indices. Assuming that the ENSO phenomenon is the source of much of the variability at these time scales, this indicates that ENSO has been an important part of interannual climatic variations over broad areas of the circum-Pacific region throughout the last millennium. Significant coherence values were found for El Niño and reconstructed Sierra Nevada winter precipitation at ~ 2–4 yr throughout much of their common record (late 1500s to present) and between 6 and 7 yr from the mid-18th to the early 20th century.

At decadal time scales each record generally tends to exhibit significant spectral power over different periods at different times. Both the Quelccaya Ice Cap $\delta^{18}O$ series and the Quinn El Niño event record exhibit significant spectral power over frequencies ~ 35 to 45 yr; however, there is low coherence between these two series at those frequencies over their common record. The Sierra Nevada winter rainfall reconstruction exhibits consistently strong variability at periods of ~ 30–60 yr.

Climatic Change **26:** 317–342, 1994.

1. Introduction

There is considerable interest in expanding our knowledge about the natural variability of climate. Such knowledge can be useful in evaluating whether recent climatic changes are unique in their spatial and temporal characteristics, or possibly reflect anthropogenic forcing. In particular, recent observational and modelling studies of ocean circulation suggest that the oceanic response to perturbations in the climate system can be both large and rather abrupt (Bryan, 1986; Manabe and Stouffer, 1988; Venrick *et al.*, 1987; Dickson *et al.*, 1988; Ebbesmeyer *et al.*, 1991; Gordon *et al.*, 1992). Stocker and Mysak (1992) have evaluated the spectral signatures of several climate indicators and suggest that the characteristic time scales of variability in these records (in the range of 50–400 yr) are indicative of low-frequency ocean-to-atmosphere heat flux variations, and they point to the North Atlantic as a potential major source of this variability.

Increased attention has been focused recently on long-term variability of the El Niño/Southern Oscillation (ENSO) phenomenon (Enfield and Cid, 1991; Quinn and Neal, 1992; Diaz and Pulwarty, 1992; Michaelsen and Thompson, 1992). ENSO represents one of the major modes of natural variability of the earth's climate system; hence, documenting long-term changes in the ENSO cycle in order to understand possible mechanisms associated with such low-frequency variations, would seem useful, not only from the point of view of detecting future anthropogenic changes in climate, but also with the aim of improving climate prediction at decadal time scales.

We have used a suite of long-term indices which are sensitive to some aspect of the ENSO phenomenon. Table I summarizes these indices, their sources, and the period of record covered. All of these indices are located in the general area of influence of the Southern Oscillation (Trenberth and Shea, 1987). One is a direct El Niño chronology developed by W. Quinn and coworkers (Quinn *et al.*, 1987, plus subsequent papers). We have used the latest version of this data set, namely that given in Quinn (1992). Five of the seven series considered here sample portions of the Medieval Warm Period ($\sim$ A.D. 950–1250). The other two begin around A.D. 1500, and are included for comparative purposes. A comparison of the temporal variability of these ENSO-sensitive indices may be useful in evaluating how different elements of the large-scale ENSO system, which have only been thoroughly documented for about the last century, may have operated over a much longer period. We are also interested in evaluating whether there are unique elements in these proxy records within the time frame associated with the Medieval Warm Period (MWP), the subject of this special issue.

Our analysis follows two main objectives. One is to describe the characteristic time scales of variability of these ENSO indicators by using the technique known as singular spectrum analysis (Vautard and Ghil, 1989; Ghil and Vautard, 1991; Vautard *et al.*, 1992) in combination with the multitaper method for calculating the spectra of each series (Thomson 1982, 1990a, b; Park *et al.*, 1987). We also

TABLE I: Sources of Proxy ENSO records used in this study. All data are annual, except where noted

	Type of Proxy index	Period of Record
1.	QEN Index. Occurrence of El niño events based on historical and other sources (Quinn *et al.*, 1987; updated in Quinn and Neal, 1992).	A.D. 1525–1985
2.	QNR Index. Compilation of the degree of severity of annual Nile River flood intensity (Quinn, 1992).	629–1520
3.	Qδ^{18}O Index. Quelccaya Ice-Cap δ^{18}O values. (Thompson and Mosley-Thompson, 1989).	744–1984
4.	SRNF Index. Reconstructed winter rainfall at Santiago, Chile (Boninsegna, 1988).	1220–1972
5.	PSTMP Index. Reconstructed summer temperatures (from tree-rings) for Rio Alerce, Argentina. (Villalba, 1990).	870–1983
6.	CD/SOI Index. Annual Chinese Drought/SOI Index (Zhang *et al.*, 1989).	1471–1985
7.	SNWR Index. Reconstructed winter precipitation in the southern Sierra Nevada, California. (Graumlich, 1993).	800–1988

evaluate the cospectrum, coherence (coherency-squared) and phase among the different spectra for evidence of temporal association at characteristic ENSO time scales and at the longer time scales. The cross-spectral measures are calculated using multitaper coherence (Thomson, 1982) with jackknifed error estimates as a measure of statistical significance (Thomson and Chave, 1991; Kuo *et al.*, 1990). A second aim is to ascertain what changes, if any, have occurred in the variance spectrum of these different indices over the past several centuries within the ENSO time scale, and at decadal to century scales where oceanic forcing of the atmosphere may be important.

2. Analysis Methods

Two nonparametric procedures, singular spectrum analysis (SSA) and Thomson's (1982) multi-taper method (MTM) are used in combination to analyze the spectrum of the various climate indices. SSA has been shown to be a useful tool for defining the principal models of variability of geophysical series. MTM has been shown to be an improvement over traditional single-window estimates (see Park *et al.*, 1987; and Thomson, 1990a).

SSA, an extension of empirical orthogonal function analysis, considers M lagged copies of a time series process x_i $1 \leq i \leq N$, sampled at equal time intervals τ_s, and calculates the eigenvalues λ_k and eigenvectors ρ_k, $1 \leq k \leq M$ of their covariance matrix $\mathbf{C}$ (see Ghil and Vautard, 1991; Vautard *et al.*, 1992). The matric $\mathbf{C}$ has a Toeplitz structure with constant diagonals corresponding to equal lags. The

choice of window width, $\tau_w = M\,\tau_s$, represents a tradeoff between the amount of information desired to be retained (large M), and statistical significance (small M). Subsets of eigenelements and associated principal components provide for noise reduction, the removal of trend and the identification of oscillatory components (Rasmusson *et al.*, 1990; Penland *et al.*, 1991; Vautard *et al.*, 1992). Selected components provide for optimal reconstruction of particular processes at precise time scales. As in spatial EOF analysis, the complete sum of all eigenelements returns the original input series. In contrast to other standard filtering techniques, where the basis functions are selected a priori, SSA functions as a data-adaptive filter.

The multi-taper method involves multiplication of the input data series by an optimal set of leakage-resistant tapers, yielding several series from one record (see Thomson 1990a, b; Park *et al.*, 1987). A discrete Fourier transform is applied to each of these series producing several 'eigenspectra'. In a single-taper direct estimate of the spectrum of a white noise process at frequency f, and bandwidth $2W$, we aim to maximize Λ, the fraction of spectral energy in that estimate that derives from the frequency interval $|f-f'| \leq W$,

$$\Lambda(N, W) = \frac{\int_{-W}^{W} |\mathrm{A}(f)|^2 df}{\int_{-1/2}^{1/2} |\mathrm{A}(f)|^2 df}\,, \tag{1}$$

where $\mathrm{A}(f)$ is the discrete Fourier transform of the data tapers, and $1-\Lambda$ is the fraction of spectral energy that leaks from outside the band. The weighted sum of the eigenspectra form a single spectral estimate with little compromise between leakage and resolved variance. The statistical information discarded by the first taper is partially recovered by the second taper, and so on. Park *et al.* (1987) and Thomson (1990a) furnish good documentation and applications of the technique.

The tapers minimize loss of information, as is the case with traditional single tapers, while also optimizing resistance to spectral leakage. Many geophysical time series exhibit nonstationary behavior with time. The multitaper method, which is designed to weigh data as evenly as possible from the full record sample, is not subject to problems associated with single taper techniques which discard varying amounts of end data, while overemphasizing signal power over the central portions of the record. The multitaper spectral estimates are a smoothed estimate, and also a consistent estimator of spectral variance. Another advantage of MTM is that the statistical significance of the spectral peaks can be calculated via an F-ratio test.

The evolution of local spectrum in time provides valuable information on the onset, amplification or disappearance of oscillatory behavior. Such behavior is associated with internal mechanisms typical of nonlinear systems (Yiou *et al.*, 1991). This 'evolutive' spectral analysis (ESA) is achieved by selecting a specified window length, calculating the spectrum within each window (via the above method), and repeating the process while moving the time window along through the series being analyzed.

The time series of event-type data – the Quinn El Niño record (QEN) and the Quinn Nile River flood-deficit series (QRN), which are made up of zeros (no event) and ones (event occurrence) – were transformed to a smoother-valued record by converting it to 'events per year' within overlapping 25-yr segments. For example, for a given 25-yr period within the overall period of record, if there were, say, five El Niño events, then the central year of that interval would have a value of 0.20 (5/25 events/yr). This also implies a mean event recurrence interval of 5 yr. To recover information on ENSO time scales, a second series (QENres) was used which consists of the difference between the original (0s and 1s) series and the 'windowed' series. The choice of window length is arbitrary and depends on the analysis objectives. In this case, the high-frequency window contains spectral power from the biennial and ENSO time scale ($\sim$ 2 to 9 yr), as well as time scales associated with solar cycle variability ($\sim$ 11 and 22 yr). This is one of two ENSO-sensitive series that lies entirely outside the MWP (the other being a reconstruction of the Tahiti-Darwin Southern Oscillation Index derived from historical flood/drought records). However, because it is a direct proxy of El Niño conditions in the upwelling regions off the west coast of tropical South America, it was deemed useful to include it for comparison purposes.

Diaz and Pulwarty (1992) analyzed the temporal characteristics of each of the two Quinn records and also compared an overlapping segment (1824–1941) using a 19-yr running window. In that study, we considered the possibility that at least part of the changes reflected in these records may be due to differences in the amount of information available in the historical record. To that end, we analyzed the spectrum of El Niño and Nile River flood-deficit events for different event strength thresholds. The differences between the early and later parts of these records, such as they exist, are not obviously related to historical details of the reconstructions, except possibly a period of more frequent El Niño events that is evident throughout much of the 19th century. Diaz and Pulwarty (1992) also analyzed the modern record of the Southern Oscillation (based on normalized Tahiti minus Darwin sea-level pressure difference since the 1880s) together with a contemporary sequence of El Niño events derived directly from sea surface temperature observations in the eastern tropical Pacific Ocean. Even over this relatively short time period there have been changes in the large-scale structure of ENSO (see Cole *et al.*, 1993). Hence, in the absence of clear evidence that temporal differences in the QEN series are due solely (or mostly) to non-climatic factors, we will proceed here by taking the data at its face value.

We note that only the moderate and stronger event classification have been used in the present study. The question of how to categorize multi-year events (such as the 1939–41 and 1991–93 episodes) is dealt with by following the same approach taken by a number of other investigators (see, Kiladis and Diaz, 1989), namely, that the first of a set of consecutive years with persistent ENSO-like anomalies is taken as year zero of that event. While it is true that other classification approaches would have the effect of changing somewhat the recurrence characteristics of the

data (see, Hocquenghem and Ortlieb, 1992), we feel we have taken a consistent approach in this analysis.

The other series used in this study that begins after the nominal end of the MWP is a reconstruction of the Southern Oscillation Index based on a long record of dryness/wetness in eastern China (see Wu and Lough, 1987; Zhang *et al.*, 1989). The influence of the Southern Oscillation on seasonal precipitation in China is substantial, although it is primarily manifested in the subtropical humid regions of eastern China, and is subject to considerable event-to-event variations. It in included here for comparison purposes as representative of an ENSO teleconnection to the monsoon regions of Asia (see Ye *et al.*, 1987).

The SSA was performed on each series using a range of window sizes to check the stability of the eigenvalues. Lag windows of $M = 25$ and $M = 150$ were chosen to isolate components with power in the 2–25 yr and 25–150 yr bands, respectively. A Mann-Kendall test (WMO, 1966) and maximum-entropy spectral analysis (Burg, 1967) were carried out on each principal component to identify probable trends and dominant spectral peak. Separate time-series can be reconstructed using only PCs carrying power in the desired bands. Furthermore, we focus specifically on pairs of adjacent PCs which correspond to oscillatory components. Each reconstructed band series is analyzed via the MTM technique, with bandwidth $W = 5/N$ and $K = 9$ tapers, where N is the length of the respective series. Multi-taper evolutive spectrum of each series is calculated using a moving window of 91 yr with increment of one year. Statistical significance via an F-ratio test is evaluated at each step and can be mapped in the same manner as the evolutive spectrum. Coherence and phase were calculated among all series pairs; however, only cross-spectra from series with significant power in similar spectral bands, and in particular within the high-frequency ENSO band, are discussed in detail below.

3. Data Analysis

3.1. *Characteristic Scales of Variation*

Standardized indices of the Quinn El Niño series (QEN) and the Quinn Nile River flood-deficit series (QNR) that have been SSA-filtered at different wavelengths are shown in Figures 1 and 2, respectively. All series have been standardized by the standard deviation of the original series to facilitate intercomparison. The amount of MTM spectral variance for each record found within the different frequency bands is listed in Table II. The amount of variance for both the transformed 25-yr filtered (QEN25/QNR25) and residual (QENres/QNRres) series are shown separately. The curves illustrate the long-period trends ($P > 150$ yr), and variability within the 25–150 year low-frequency window and in the 2–10 yr time scale. For QEN25, the amount of variance in the 25–150 yr band is 63% compared with 34% for the QNR25 data. Fluctuations at $P > 150$ yr account for three times as much of the corresponding series variance in the Nile River data than for the El Niño (66 versus

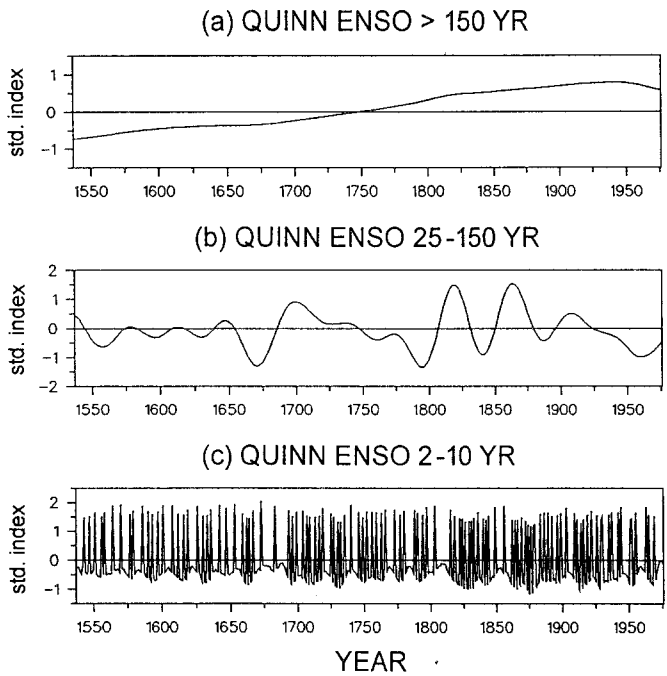

Fig. 1. Band-pass filtered series of the Quinn El Niño (QEN) record (moderate and stronger El Niño occurrence) based on a 25 yr window: (a) low frequency ($P > 150$ yr) component; (b) intermediate ($P \sim 25$–150 yr) time scales; and (c) ENSO time scale ($P \sim 2$–10 yr). Time series in (c) derived from the residual values obtained by differencing the 25-yr running window values obtained from the original data of 0s and 1s. The series were reconstructed by using the appropriate SSA principal components corresponding to the indicated time scale. Ordinate units are in standard deviations of the original series. Data from Quinn (1992).

TABLE II: Percent of variance within indicated frequency bands for each series identified in Table I. Spectrum calculated using the MTM technique on SSA-derived PCs. QEN25 and QNR25 are the transformed Quinn El Niño and Nile River series, respectively, while QENres and QNRres stand for the differenced (original minus QEN25/QNR25) series

		Frequency band			
	Index	> 150 yr	25–150 yr	< 25 yr	2–10 yr
1.	QEN25	21.0	63.0	16.0	–
	QENres	0.0	3.5	96.5	95.0
2.	QNR25	66.0	34.0	0.0	–
	QNRres	0.0	3.0	97.0	78.0
3.	$Q\delta^{18}O$	12.0	17.0	71.0	48.0
4.	SRNF	3.3	9.0	88.0	67.0
5.	PSTMP	2.2	2.2	95.6	72.0
6.	CD/SOI	0.0	8.0	92.0	85.0
7.	SNWR	2.0	7.0	91.0	71.0

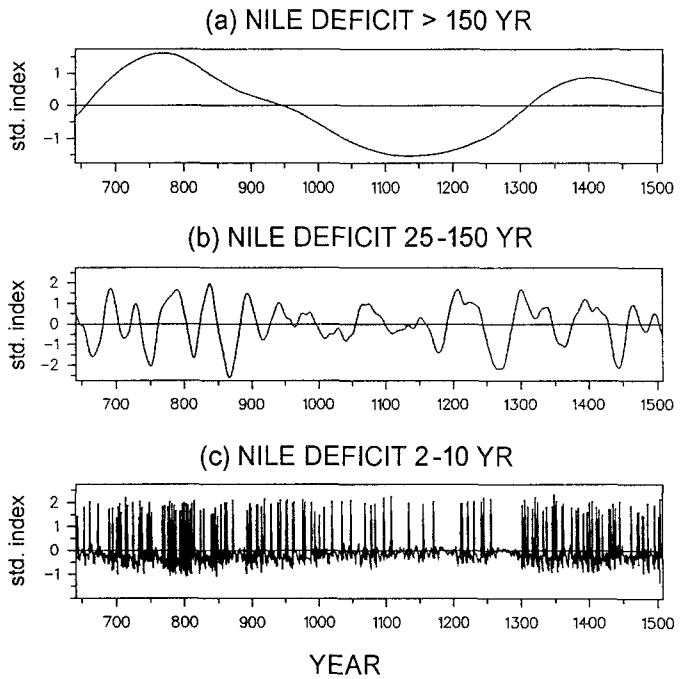

Fig. 2. As in Figure 1, but for the Nile River flood deficit record (QNR) of Quinn (1992). Events in the strongest four categories were used.

21%). In the high frequency band, about 95% of the QEN variability occurs on time scales < 10 yr compared to about 78% for QNR (Table II).

Another notable feature evident in Figures 1 and 2 is a general increase in the frequency of El Niño events over the period of record. To some extent this is likely due to improved sources of information on the South American coast with time. In the absence of other independent records of ENSO activity, such as tropical corals (Cole *et al.*, 1992, 1993), we cannot say for sure if this is entirely an artefact or a real climatic signal. By contrast, the Nile River record shows a period of low variability (few recorded instances of the occurrence of significant deficits) during the MWP, particularly in the 12th century. This can also be noted at intermediate frequencies (Figure 2b), where the amplitude of the oscillations is much reduced during that time.

Michaelsen and Thompson (1992) have shown that the $\delta^{18}O$ record from the Quelccaya Ice Cap in Peru ($Q\delta^{18}O$) has significant variance within the ENSO time scale. The actual data series, together with the low-order trend, and the decadal and higher-frequency filtered series are shown in Figure 3. About 71% of the variance is contained at $P < 25$ yr (see Table II), of which about half is contained on 2–10 yr time scale. The $Q\delta^{18}O$ record displays lower variability and some relatively high values (warmer temperatures) around 1100 A.D. However, the largest signal is associated with a cold period that extends from about the 16th through 19th

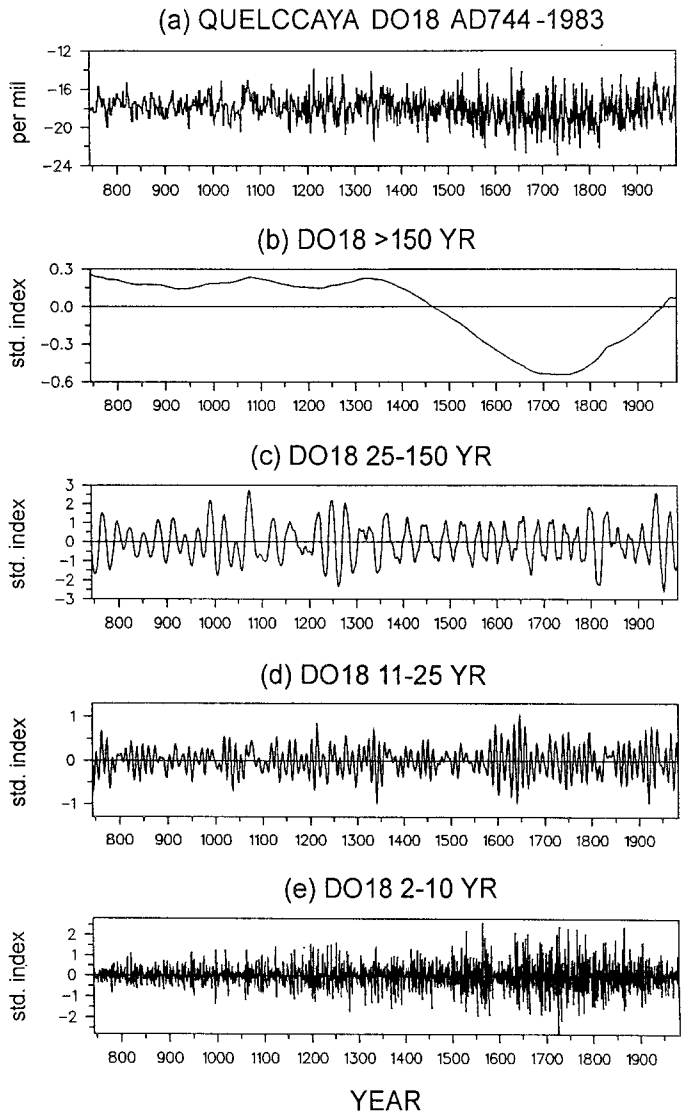

Fig. 3. Original and filtered values of the oxygen isotope ($Q\delta^{18}O$) index for the Quelccaya Ice Cap. Top panel (a) shows the unfiltered data (in units of per mill); panel (b) depicts the lowest frequency trends ($P > 150$ yr); panel (c) depicts variability within the 25–150 time scale; panel (d) shows variability at 10–25 time scales; and panel (e) variability in the 2–10 yr time ENSO band. Data provided by L. Thompson.

centuries, punctuated by greater variability at higher frequencies (Figures 3d and e). This period of sustained negative $\delta^{18}O$ anomalies falls within the time interval commonly referred to as the Little Ice Age (Grove, 1988). About 17% of the variance in the $Q\delta^{18}O$ record is found at intermediate frequencies. Except for a period of relatively high oscillations in the 13th century, we do not see anything

notable during the MWP at this time scale. The strongest spectral peak in this band occurs around 30 yr, and explains 2–3% of the total variance in the data.

Two ENSO-sensitive paleoclimate series from South America are reconstructed Santiago de Chile winter rainfall (SRNF) (Boninsegna, 1988), and reconstructed summer temperatures from northern Patagonia in Argentina (PSTMP) (Villalba, 1990). Villalba (this issue, pp. 183–197) has analyzed in detail the association between these two reconstructions and measures of ENSO variability. Here, we will restrict ourselves to an analysis of the characteristic time scales of variability in these two series and whether the association with ENSO, in terms of its main spectral features, has changed over time. Figures 4 and 5 give, respectively, the actual reconstruction, the low-order trends, decadal (25–150 yr), and higher frequency (2–25 yr) variability for SRNF and PSTMP.

The fraction of total variance contained in the ENSO band (2–10 yr) is high – about 67% and 72% for SRNF and PSTMP, respectively. Relatively little variance is found at periods greater than 25 yr (Table II). At least some of the suppression in variance at lower frequencies may be a result of the standardization procedures used in reconstructing the index. During the MWP, reconstructed summer temperatures where at their highest levels compared to the rest of the record (best illustrated in Figure 5b). Variability may also have been higher during these early centuries, although it is difficult to say for sure, since the number of chronologies varies with time, which could affect the variance near the end of such series (see review by Hughes and Diaz, this issue, pp. 109–142). Winter rainfall at Santiago, which is known to be modulated by the ENSO phenomenon (Aceituno, 1988; Kiladis and Diaz, 1989), was lowest during the 14th century, but this was followed by a peak in the 15th century. Although this series starts in A.D. 1220, and hence can not shed any light on possible changes in ENSO frequency during the early part of the MWP proper, the record is useful in that it bridges the gap between the end of the MWP and the start of the El Niño record of Quinn *et al.* (1987). Indeed, the couple of centuries preceding the start of the QEN record appear to have been somewhat unusual.

The SOI reconstruction based on a long record of floods and drought in China (CD/SOI) (Zhang *et al.*, 1989) is presented in Figure 6. Almost all the variance in this series is contained in the 2–10 yr band (Table II). No significant trend was found for this series, so it is likely that trend removal was part of the reconstruction methodology. Significant spectral peaks are found at $\sim$ 3–5 yr, and at $\sim$ 10–11 yr. A variance peak at $\sim$ 75–90 yr is evident in the first half of the record.

The last reconstruction examined consists of a 1000-year record of winter (October-June) precipitation in the Sierra Nevada Mountains of central California (SNWR, Graumlich, 1993). As there is little variance present on time scales > 150 yr (Table II), we show only the series associated with time scales from 2 to 150 yr (Figure 7). There are no notable differences in this record during the MWP compared to other parts of the record, except possibly the presence of some high amplitude variations at frequencies between $\sim$ 13–15 yr and from $\sim$ 35–60 yr.

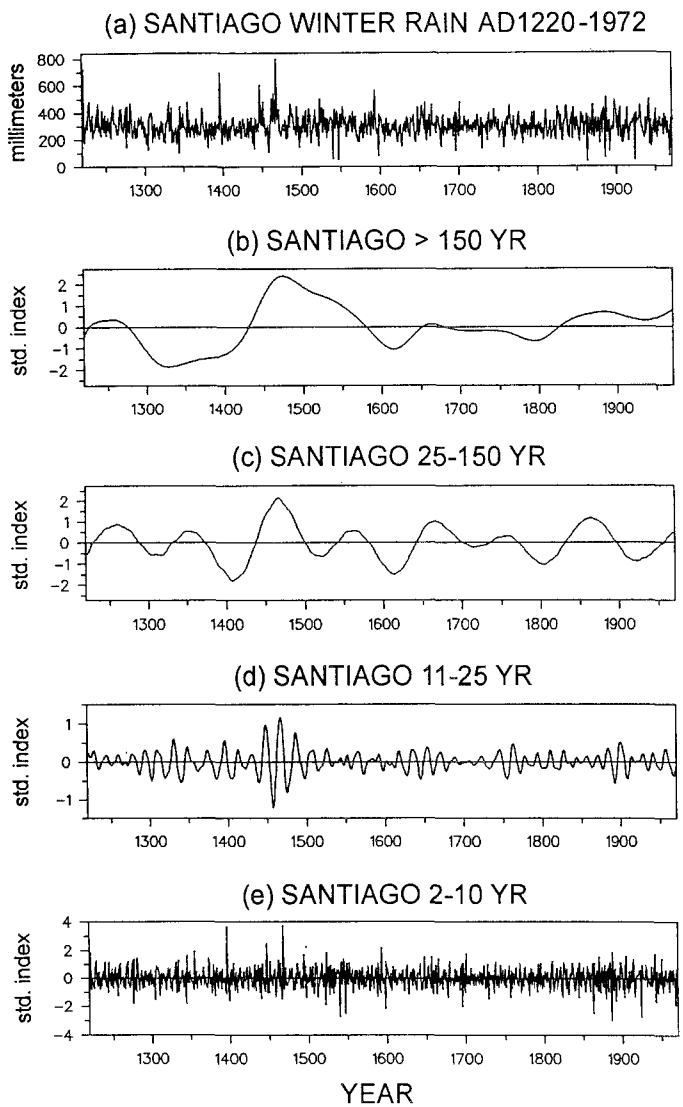

Fig. 4. As in Figure 3, except for reconstructed Santiago de Chile winter rainfall (index SRNF). Values in panel (a) are in mm. Data furnished by R. Villalba.

A separate reconstruction of growing-season temperature (Graumlich, 1993) does indicate the presence of warmer decades during the centuries spanning the MWP (see Hughes and Diaz, this issue, pp. 109–142), as well as cooler conditions from the 16th to the mid-19th century, in agreement with previous tree-ring reconstructions in this region (Briffa *et al.*, 1992). The variations illustrated in Figure 7b exhibit fairly consistent power in the frequency range from 35 to 60 yr. About 30% of the total variance in this band is associated with these time scales. An evolutive spectral analysis plot for this frequency band (Figure 8) illustrates the general strength of

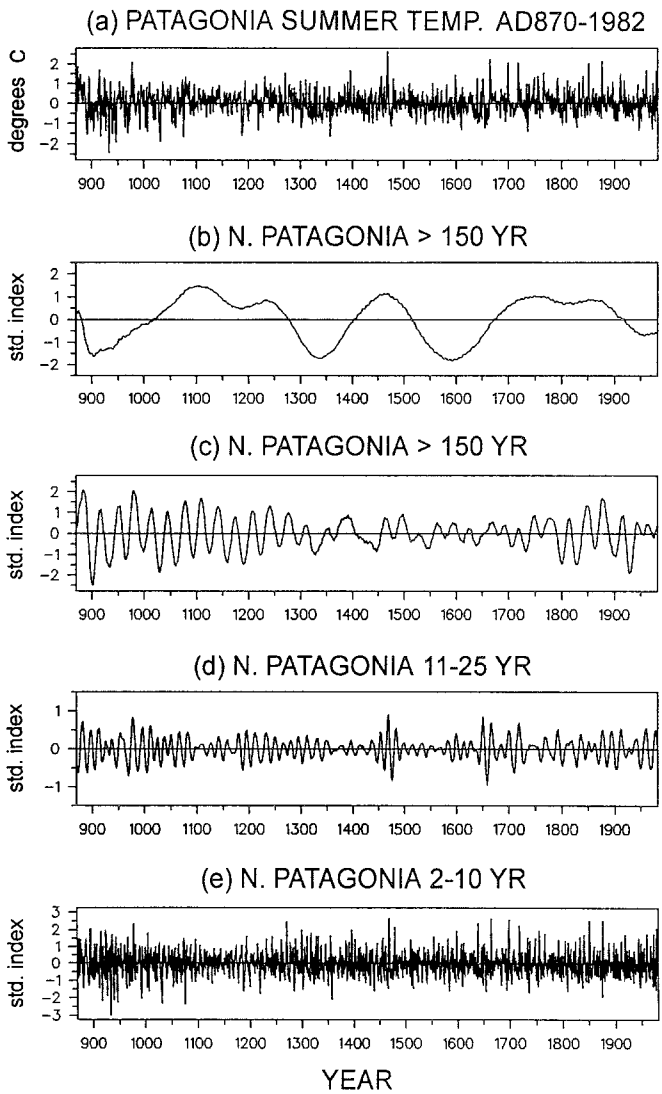

Fig. 5. As in Figure 3, except for reconstructed northern Patagonia summer temperature (index PSTMP). Values in panel (a) are in degrees Celsius. Data furnished by R. Villalba.

this signal. The high amplitude peaks shown in Figure 7b between about 1000 and 1200 A.D. are associated with oscillations having periods ~ 50–60 yr. After about A.D. 1700, the dominant fluctuations in this band occur at around 35 yr.

We next consider changes with time of the significant spectra within the 2–10 yr frequency band associated with ENSO forcing.

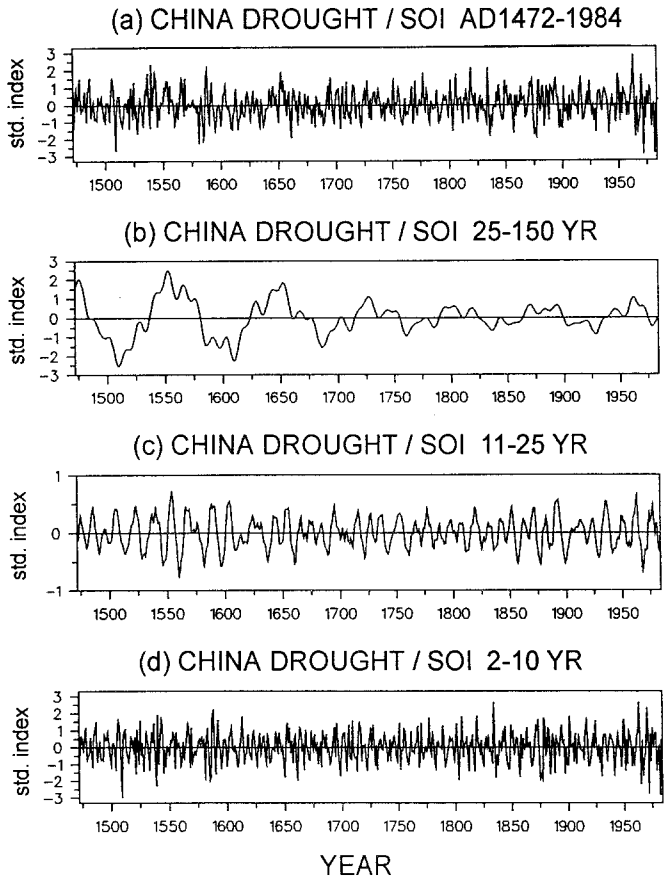

Fig. 6. As in Figure 3, except for reconstructed SOI based on Chinese drought records (index CD/SOI). Shown are (a) the actual data (originally in standardized units); (b) a filtered series tuned to highlight the variability in the 25–150 yr time scale; (c) the variability in the 10–25 yr time scales; and (d) variability in the 2–10 yr ENSO band.

3.2. *Evolutive Spectra*

Figure 9 displays the evolutive spectral signatures of the statistically significant ($\geq$ 95% confidence level) spectral components for the 2–10 year frequency band for each time series. The pluses, visible in Figure 9 as thicker line segments, denote times when variations at the particular frequency in each evolutive time step exceed 5% of the total variance. Since the emphasis in this study is on the ENSO time scale, and because of space constraints, only the ESA for the high-frequency band (specifically in the 2–10 yr window) is shown. Variance peaks at lower frequencies are discussed as appropriate. We caution the reader that changes in the spectrum of the event data imply a change strictly in the frequency of recurrence, whereas a change in the spectrum of the other series implies a modulation in the time scale of variability in the intrinsic property of the data itself.

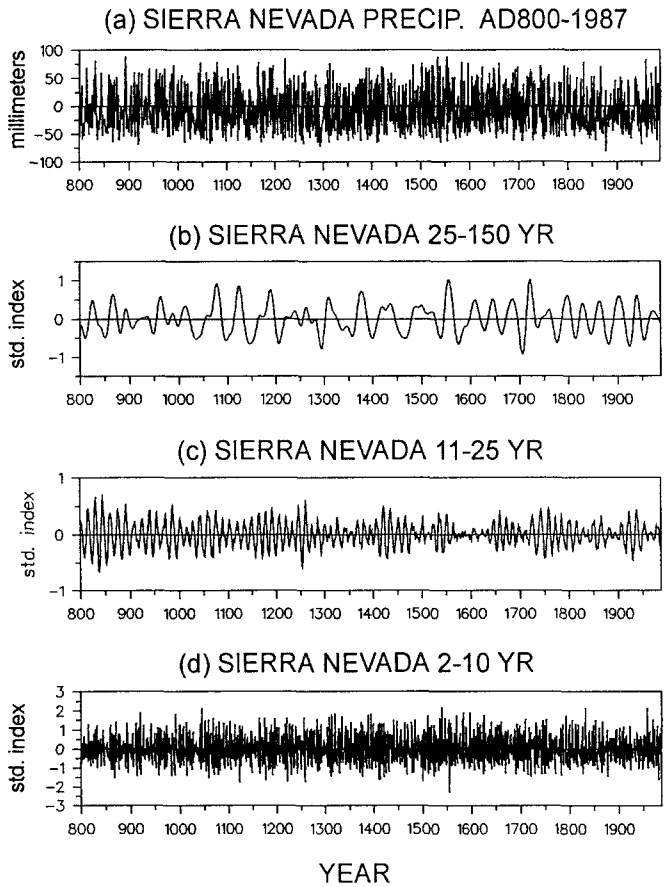

Fig. 7. As in Figure 3, except for reconstructed winter (October-June) precipitation in the Sierra Nevada mountains of central California (index SNWR). Data from Graumlich (1993), furnished by M. Hughes. Shown are (a) the actual data (in mm); (b) a filtered series tuned to highlight the variability at 25–150 yr; (c) 10–25 yr time scale; and (d) variability in the 2–10 yr ENSO band.

As expected, significant power is indicated in the canonical ENSO time scale ($\sim$ 2–6 yr) for the QENres index (Figure 9a). At lower frequency (QEN25 index) spectral peaks occur at $\sim$ 40–60 yr (evolutive spectrum not shown, see Diaz and Pulwarty, 1992). From the late 1700s to the end of the 19th century, the QEN record exhibits strong variance at $\sim$ 45 yr (see Figure 1b). Similarly, QNRres index displays significant power between $\sim$ 2–4 yr throughout most of the record (Figure 9b), but significant low frequency power occurs in different parts of the record for periods of $\sim$ 40–60 yr and near 90 yr (not shown). We should note that the residual indices, QENres and QNRres, of necessity, must contain a large amount of spectral power at frequencies characteristic of the recurrence time in the original series. However, whether the peak is at the longer ENSO time scale (> 5 yr) or at shorter periods ($\sim$ 3–5 yr) depends on the actual record of El Niño

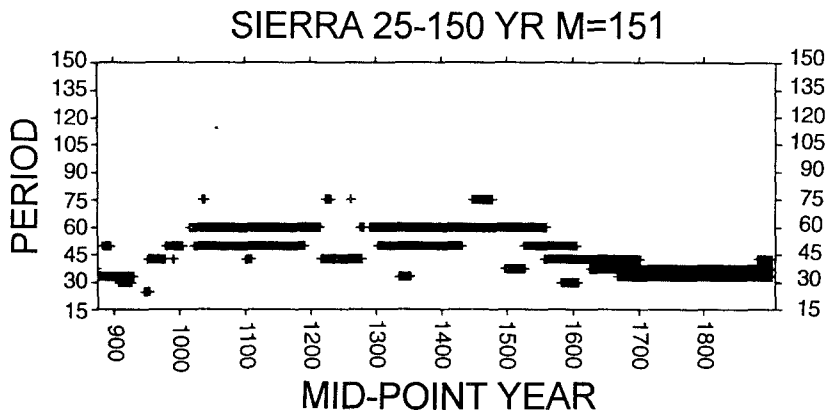

Fig. 8. Evolutive spectral analysis (ESA) for SNWR in the 25–150 yr frequency band.

occurences.

The oxygen isotope record ($Q\delta^{18}O$) exhibits a broader spectral signature with significant power throughout the ENSO band (Figure 9c) and also in the 9–14 yr time scale (see Figure 3). During the MWP, variations in the $Q\delta^{18}O$ record appear to be concentrated at relatively longer periods in the ENSO band ($\sim$ 5–8 yr), whereas later on they occur mostly at somewhat higher frequencies, between $\sim$ 2–6 yr. Significant and continuous power is also found at $\sim$ 25–50 yr (not shown, but see Figure 3c). An increase in negative $\delta^{18}O$ ratios is evident during the Little Ice Age ($\sim$ A.D. 1500–1900). During that time $\delta^{18}O$ variations had a strong rhythm at $\sim$ 30 yr.

The corresponding ESA for SRNF is given in Figure 9d. At higher frequencies, significant and continuous power is evident at $\sim$ 8 yr and between about 2 and 6 yr, and also from $\sim$ 16–22 yr (not shown). Before about A.D. 1500 there are no dominant frequencies at the 2–10 yr time scale, but after about A.D. 1600, variability at $\sim$ 3–4 yr is strong. At the lower frequencies, two harmonics stand out, one at $\sim$ 94 yr, and a second at $\sim$ 125 yr. For northern Patagonia summer temperatures (Figure 9e), consistent variance peaks are found at $\sim$ 3–6 yr, near 10 yr, and a strongly continuous peak is found near $\sim$ 25–40 yr in the 25–150 yr band (not shown).

The principal time scale of variability for the CD/SOI index is concentrated in two narrow bandwidths – between $\sim$ 4–6 yr, and, after 1800, between $\sim$ 7–8 yr as well (Figure 9f). As noted earlier, there is little low frequency variance associated with this index, although a relative peak is found at $\sim$ 70—85 yr periods in the first half of the record (Figure 6b). Lastly, the Sierra Nevada winter precipitation index, exhibits strong variability at $\sim$ 2–5 yr and from $\sim$ 6–8 yr (Figure 9g). It was noted earlier that at lower frequencies, the strongest spectral signatures occur between 35 and 60 yr, with a weaker one near 100 yr.

Table III provides a summary of the principal spectral lines in the 2–10 yr

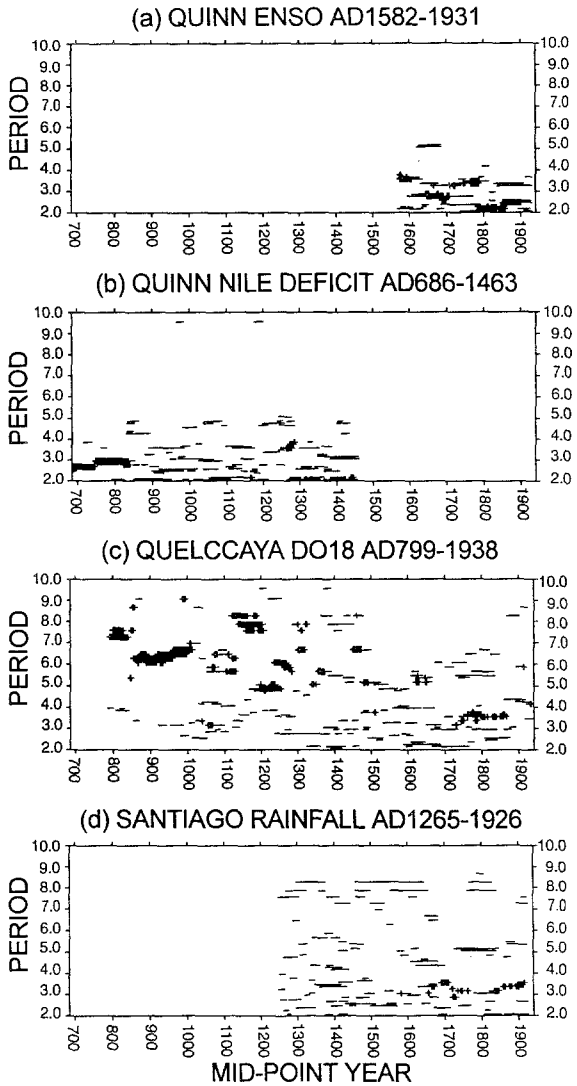

Fig. 9. Evolutive spectral analysis (ESA) for different indices: (a) QENres; (b) QNRres; (c)Qδ^{18}O; (d) SRNF; (e)PSTMP; (f)CD/SOI; (g) SNWR in the 2–10 yr spectral band. Two symbols are used, a straight line for values that account for less than 5% of the total variance in the data and pluses (+) to denote 91-yr segments when the line spectra account for more than 5% of the data variance in that particular segment. Only components significant at the 95% confidence level are shown.

frequency band (column labelled LINES). It also lists the periods where significant coherence peaks are found among the different series. The coherence features are discussed further below. The significant spectral peaks occur at frequencies near the tropical quasi-biennial oscillation (QBO), near the mean recurrence frequency for ENSO events (3–4 yr) and at periods in the neighborhood of 6 yr.

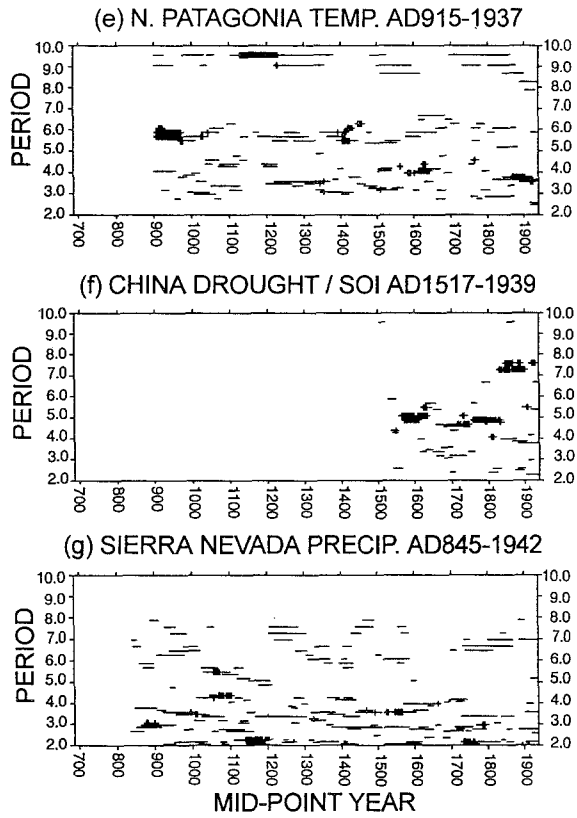

Fig. 9. (continued)

To further illustrate the persistence of the major periods found in these long-term ENSO indices, Figure 10 illustrates the fraction of time where a significant spectral peak has been plotted in Figure 9. For comparison, the corresponding fractions of time where significant spectral peaks are found within the MWP are included. Only the five series containing data in the MWP are shown. The Nile (QNRres) and Sierra Nevada (SNWR) indices (Figure 10a and e) display consistent oscillations in the 2–4 yr time scale throughout their respective periods of record. The $Q\delta^{18}O$ series exhibits relative low percentages before $\sim$ 5 yr, but consistent variability from about 5 to 9 yr (Figure 10b). Northern Patagonia summer temperature (PSTMP) exhibits consistent variance peaks around 5.7 and 9.7 yr, while the Santiago, Chile reconstruction (SRNF) exhibits a persistent variance peak around 8.1 yr (Figure 10c and d).

3.3. *Coherence Spectra*

One purpose of this study was to ascertain the degree of coherence among the various series within the ENSO time scale, and the stability of these relationships

TABLE III: Oscillatory components obtained via SSA (LINES col.) and significant coherence spectra at the indicated harmonics which correspond to periods where both series have significant variance spectrum components at the 90 and 95% (bold figures) significance levels

	LINES	Qδ^{18}O	SRNF	PSTMP	CD/SOI	SNWR
QENres	**2.2, 2.8, 3.3, 6.7**	**2.2, 5.7**	3.3, **4.5** 6.6	2.2, **3.3** 6.1	2.8, **5.9**	**2.2**, 2.9, 6.7
QNRres	**2.2, 2.9, 3.6**	**2.4**, 3.6	3.8,	**2.4**, 3.4, 8.1		**2.2**, 6.7
Qδ^{18}O	**2.2, 3.6, 6.4**		**3.8, 3.4** 4.1, 8.1	2.2, **4.4** 6.5	**3.4, 4.1** 9.1	**2.2**, 3.1, 5.9, **7.5**
SRNF	**2.9, 3.4, 8.1**			**2.4, 6.1** 4.8	**3.4, 4.1**	**2.6, 3.4,** 7.4
PSTMP	**3.8, 5.7, 8.5, 9.7**				**2.2**, 3.5 **4.2**	**2.7**, 4.8
CD/SOI	**2.4, 4.9, 7.5**					**2.4**, 3.4 **5.4**
SNWR	**2.2, 3.6, 6.7**					

over time. We have calculated coherence spectra using the method outlined in Thomson (1982) and Thomson and Chave (1991), and have applied that method in an evolutive fashion as described earlier. Figure 11 shows squared coherency spectra in the 2–10 yr ENSO band for selected pairs of indices. Panels 11a–d show the coherency-squared and phase between the QENres and the Qδ^{18}O, SRNF, PSTMP, and SNWR, indices, respectively. The Quinn El Niño record was used as the reference series, since this is the only one of the seven series used here that can be considered to be a 'true' index of ENSO activity (the other locations being forced by ENSO variability through teleconnection processes). Although the QEN series, unfortunately does not extend back to the MWP, we feel that some insight can be gained by comparing the behavior of the different series through a span of more than four centuries.

The highest coherence values between the QENres and Qδ^{18}O series (all significant at between 95 and 99% confidence levels) occur in the frequency band from 5 to 6 yr (Figure 11a), with the QENres series leading the Qδ^{18}O by 2 to 3 months at $\sim$ 5.7 yr (Table III). Typically, oxygen isotopic ratios are less negative (indicative of warmer prevailing conditions) in association with major warm events of the Southern Oscillation. At the same time, the accumulation record indicates lower precipitation values during El Niño years. The peak in the annual cycle of precipitation in this region of the Peruvian Andes occurs during northern spring. The reader is referred to Thompson and Mosley-Thompson (1989) for particulars of the ice core record on the Quelccaya Ice Cap.

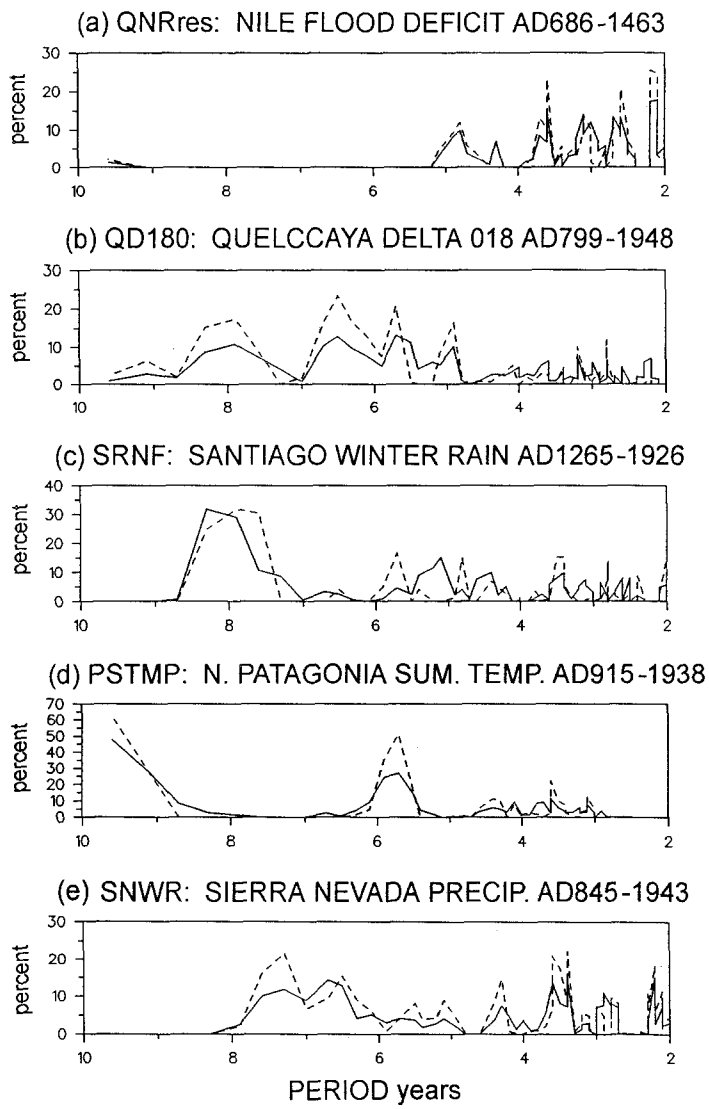

Fig. 10. Percentage of time that a significant line spectra is found in the evolutive spectrum of (a) QENres; (b) Qδ^{18}O; (c) SRNF; (d)PSTMP; and (e) SNWR over the full period of record (solid line) and within the MWP (A.D. 900–1400, dashed line).

By and large, we find strong coherence between the Quinn El Niño (QENres) series and the other series within the ENSO time scale of ~ 2–6 yr. The coherence spectra between QENres and SRNF is also interesting. In the statistically significant band near 4 yr (Figure 11b), SRNF leads QENres by about 4 months, which is roughly what is observed today, as winter (June-August) rainfall in Santiago de Chile tends to be above normal during a developing El Niño, several months before the event reaches a peak along the Peruvian coast (Kiladis and Diaz, 1989).

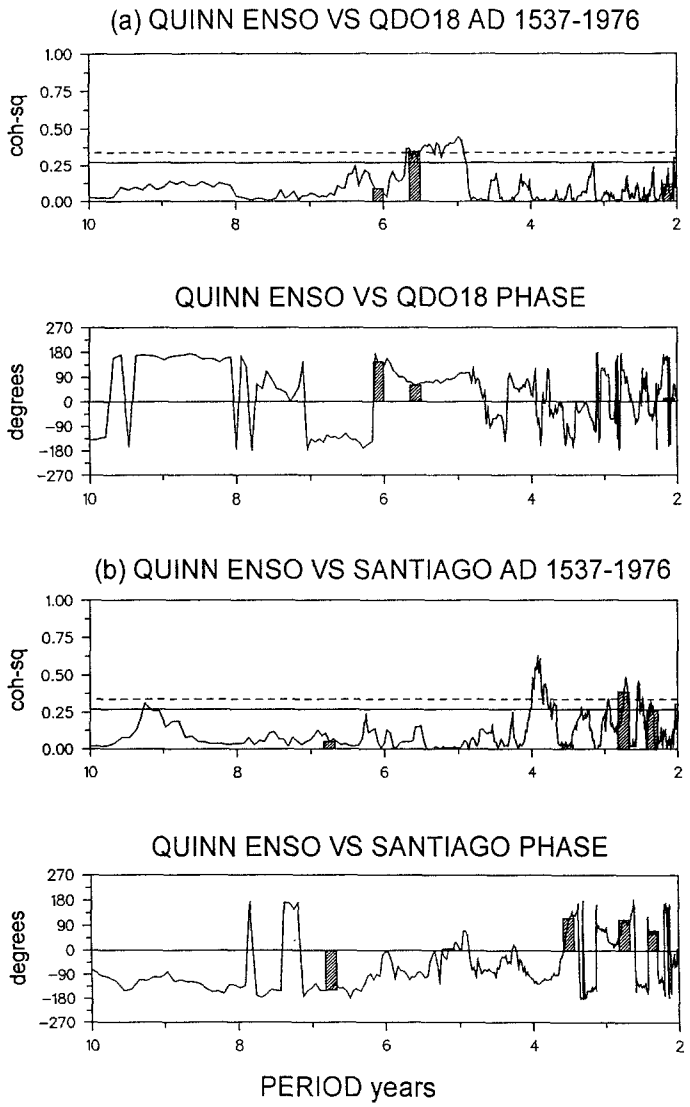

Fig. 11. Coherency-squared and phase calculated for the 2–10 yr ENSO frequency band. Solid and dashed horizontal lines denote 95% and 99% significance levels, respectively. Panel (a) QENres vs Qδ^{18}O; (b) QENres vs SRNF; (c) QENres vs PSTMP; and QENres vs CD/SOI. Vertical shaded bars highlight frequencies that exhibit oscillatory components in the autospectra of both series (see Table III). The height of the bar corresponds to the coherency and phase value at the particular point in the respective plot.

The coherence spectra for QENres and Patagonia summer (December-April) temperature reconstruction (PSTMP, Figure 11c) exhibit major peaks at 3.3, 4, and 6 yr, with the El Niño index leading by about four months in each instance. Three significant coherency peaks, in the frequency interval from $\sim$ 2 to 4 yr periods, are evident between QENres and SNWR (Figure 11d). The phase is different for each

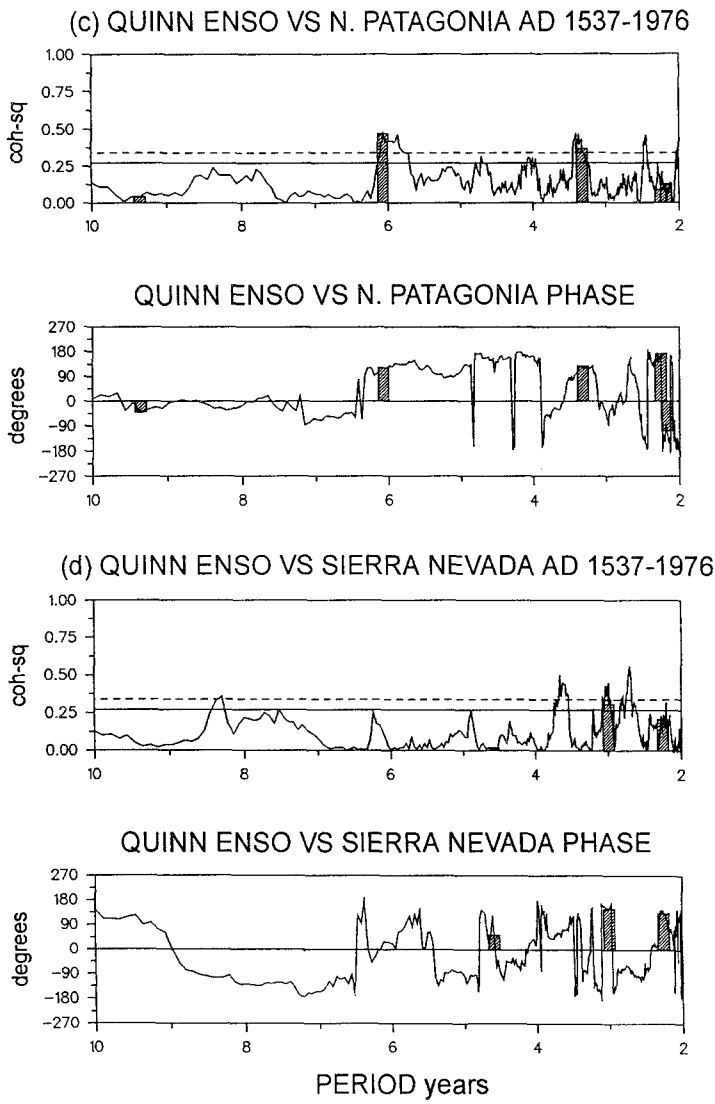

Fig. 11. (continued)

peak, but for the one around 3.7 yr, which is close to the long-term mean El Niño recurrence in the modern record, QNRres leads SNWR by about two months.

Highly statistically significant coherence peaks between QENres and CD/SOI are found between 2 and 3 yr, and around 6 yr (figure not shown), with QNRres leading by about 3 months. High coherence is found between CD/SOI and SRNF in the $\sim$ 2–4 yr band (figure not shown), but only the peaks between 3 and 4 yr are consistent with an ENSO-type signal, as SRNF is below normal when the reconstructed SOI is high (La Niña conditions) and viceversa for low SOI values (El Niño conditions). Indeed, what these analyses show is that the ENSO signal,

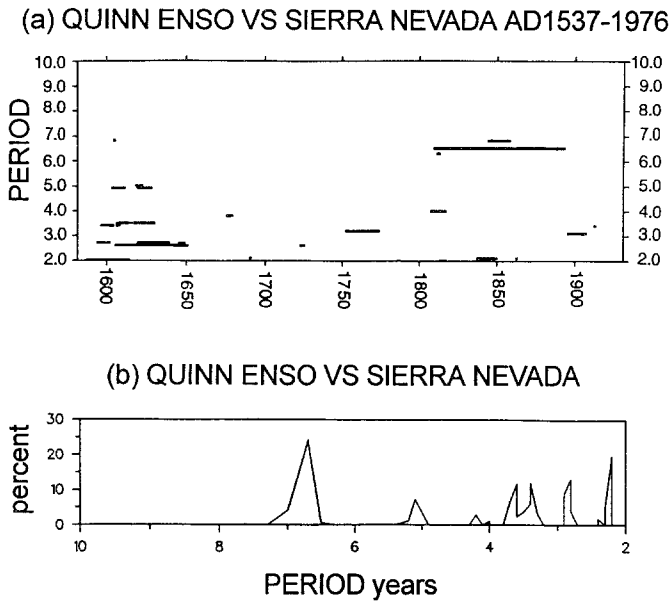

Fig. 12. Evolutive coherence between QENres and SNWR, (a) coherence-squared at 90% significance level, with the stipulation that both individual peaks must also be significant at the 90% level; (b) percentage of time that a significant coherency value is plotted in (a).

as reflected in variations in the frequency of recurrence of the event data, and in amplitude/frequency variations in the continuous records, is reasonably well manifested in the coherence spectra among the series.

We calculated the evolutionary coherence spectrum for the different series pairs within the 2–10 yr ENSO frequency band. However, unlike the ESA of the autospectra, the persistence of the significant coherence peaks through time is considerably lower. In general, significant peaks occur only over short time intervals. One of the most consistent cospectra is between QENres and SNWR (Figure 12). Here, ENSO covariability is fairly well preserved around 3–4 and 6–7 yr. The lower panel shows the percent of time the coherency is significant in the 91–yr running window at the 90% confidence level.

4. Summary and Discussion

The band-specific behavior of a suite of long period temperature and precipitation indices were examined. These indices covered a broad zone around the Pacific centers of action of the Southern Oscillation and have previously been shown to be sensitive indicators of climatic effects associated with the changing phases of the SO. Our aim was to describe the basic temporal characteristics of these ENSO-sensitive time series, and to ascertain if the variability in these records on time scales pertinent to the ENSO phenomenon was consistent throughout the past several centuries. To accomplish these goals, we have used the techniques

TABLE IV: Summary listing of significant spectral peaks in the SSA/filtered time series described in Table I.

	Index	High-frequency peaks	Low-frequency peaks
1.	QEN	~2–6 yr	~40–60 yr
2.	QNR	~2–5 yr	~40–60 yr; ~90 yr
3.	$Q\delta^{18}O$	~2–8 yr; 9–14 yr	~25–50 yr
4.	SRNF	~8 yr; 16–22 yr	~94 & 125 yr
5.	PSTMP	~3–6 yr; ~10 yr	not significant
6.	CD/SOI	~3–8 yr	~70–85 yr
7.	SNWR	~2–8 yr	~35–60 & 100 yr

of singular spectrum analysis (SSA) in combination with the multitaper methods (MTM) of spectral estimation.

Table IV summarizes the principal time scales of variability in the seven ENSO-sensitive indices analyzed in this study. For nearly all the indices, we found consistent, significant spectral peaks in the frequency band from ~ 2–6 yr, which encompasses both the biennial and ENSO time scales. Spectral coherence between the indices at these frequencies was generally significant. Temporally coherent spectral power at intermediate frequencies (~ 25–150 yr) was also found, although coherence among the various indices at this frequency range was typically low. A few of the series also exhibited very low frequency (> 150 yr) behavior whose authenticity is unknown. Within the time interval encompassed by the Medieval Warm Period (here broadly defined as ~ 900–1400 A.D.), only the Nile River flood-deficit record and the northern Patagonia summer temperature index appear to show extraordinary behavior. In the former case, much lower incidences of Nile flood deficits are recorded, whereas for the latter, warmer summers are indicated. The Sierra Nevada record exhibits a period of large precipitation fluctuations lasting about one to two centuries. The summer temperature record derived from tree-ring data at the same site does indicate warmer summer during the MWP (Graumlich, 1993, see also Hughes and Diaz, this issue, pp. 109–142). The $\delta^{18}O$ record also exhibits a marked dip (cooler temperatures) during the core of the Little Ice Age.

It appears that the climatic variability expressed at the ENSO time scale is retained quite consistently in nearly all of these climate-sensitive records (of course, the QEN series is implictly a record of El Niño occurrences on the South America Pacific coast). Low frequency behavior of the QEN series has been previously documented (Enfield and Cid, 1991; Diaz and Pulwarty, 1992), and additional high-resolution (annual or seasonal) ENSO-sensitive indices are becoming available for studying low frequency variations in the ENSO system (Cole *et al.*, 1992, 1993). Given the limited sampling available during the MWP, the results of our study suggest that there were not major differences in the climatic expression of the ENSO phenomenon during the last millenia, a period encompassing a warm epoch

(at least regionally, see a review by Hughes and Diaz, this issue, pp. 109–142) and a generally colder period (the 'Little Ice Age'). Enfield (1992) and Nicholls (1992), on the basis of various lines of evidence, both argue for a relatively stable ENSO system. Although modulations in the relationship between El Niño and the Southern Oscillation have been documented for about the past century (Trenberth and Shea, 1987; Deser and Wallace, 1987; Cole *et al.*, 1993), and other studies suggest differences over longer periods (see Diaz and Markgraf, 1992), it appears that ENSO may have operated in a substantially similar fashion over the past thousand years as it has during the past century.

Acknowledgements

We wish to thank Lisa Graumlich and Ricardo Villalba for making their tree-ring reconstructions available to us. Villalba also kindly provided Boninsegna's reconstruction for Santiago de Chile rainfall (that record is discussed in a book edited by Bradley and Jones (1992). Records for the other sites were obtained from the published sources. We also thank the two reviewers for their valuable comments which helped to improve the manuscript.

References

Aceituno, P.: 1988, 'On the Functioning of the Southern Oscillation in the South American Sector', *Mon. Wea. Rev.* **116**, 505–524.

Boninsegna, J. A.: 1988, 'Santiago de Chile Winter Rainfall since 1220 as Being Reconstructed by Tree-Rings', *Quatern. South Amer. Antarc. Penins.* **6**, 67–87.

Bradley, R. S. and Jones, P. D. (eds.): 1992b, *Climate Since A.D. 1500,* Routledge, London and New York, 679 pp.

Briffa, K. R., Jones, P. D., and Schweingruber, F. H.: 1992, 'Tree-Ring Density Reconstructions of Summer Temperature across Western North America', *J. Clim.* **5**, 735–754.

Bryan, F.: 1986, 'High-Latitude Salinity Effects and Interhemispheric Thermohaline Circulation', *Nature* **323**, 301–304.

Burg, J. P.: 1967, 'Maximum entropy spectral analysis', Reprinted in *Modern Spectrum Analysis* (1978), D. G. Childers (ed.), IEEE Press, NY, pp. 42–48.

Cole, J. E., Shen, G. T., Fairbanks, R. G., and Moore, M.: 1992, 'Coral Monitors of El Niño/Southern Oscillation Dynamics across the Equatorial Pacific', in Diaz, H. F. and Markgraf, V. (eds.), *El Niño: Historical and Paleoclimatic Aspects of the Southern Oscillation*, Cambridge University Press, Cambridge, pp. 349–375.

Cole, J. E. Fairbanks, R. G., and Shen, G. T.: 1993, 'Recent Variability in the Southern Oscillation: Isotopic Results from a Tarawa Atoll Coral', *Science* **260**, 1790–1793.

Deser, C. and Wallace, J. M.: 1987, 'El Niño Events and Their Relation to the Southern Oscillation: 1925–1986', *J. Geophys. Res.* **92**, 14,189–14,196.

Diaz, H. F. and Markgraf, V.: 1992, *El Niño: Historical and Paleoclimatic Aspects of the Southern Oscillation*, Cambridge University Press, Cambridge, 476 pp.

Diaz, H. F. and Pulwarty, R. S.: 1992, 'A Comparison of Southern Oscillation and El Niño Signals in the Tropics', in Diaz, H. F. and Marktraf, V. (eds.), *El Niño: Historical and Paleoclimatic Aspects of the Southern Oscillation*, Cambridge Univesity Press, Cambridge, pp. 175–192.

Dickson, R. R., Meincke, J., Malmberg, S. -A., and Lee, A. J.: 1988, 'The "Great Salinity Anomaly" in the Northern North Atlantic 1968–1982', *Prog. Oceanogr.* **20**, 103–151.

Ebbesmeyer, C. C., Cayan, D. R., McLain, D. R., Nichols, F. H., Peterson, D. H., and Redmond, K. T.: 1991, '1976 Step in the Pacific Climate: Forty Environmental Changes between 1968–1975 and 19770–1984', *Proc. Seventh Ann. Pacific Climate (PACLIM) Workshop*, California Dept. of Water Resources.

Enfield, D. B.: 1992, 'Historical and Prehistorical Overview of the El Niño/Southern Oscillation', in Diaz, H. F. and Markgraf, V. (eds.), *El Niño: Historical and Paleoclimatic Aspects of the Southern Oscillation*, Cambridge University Press, Cambridge, pp. 95–117.

Enfield, D. B. and Cid S., L.: 1991, 'Low-Frequency Changes in El Niño-Southern Oscillation', *J. Clim.* **4**, 1137–1146.

Ghil, M. and Vautard, R.: 1991, 'Interdecadal Oscillations and the Warming Trend in Global Temperature Time Series', *Nature* **350**, 324–327.

Gordon, A. L., Zebiak, S. E., and Bryan, K.: 1992, 'Climate Variability and the Atlantic Ocean', *EOS* **73**, 161–165.

Graumlich, L. J.: 1993, 'A 1000-Year Record of Temperature and Precipitation in the Sierra Nevada', *Quatern. Res.* **39**, 249–255.

Grove, J. M.: 1988, *The Little Ice Age*, Methuen, London and New York.

Hocquenghem, A. -M. and Ortlieb, L.: 1992, 'Historical Record of El Niño Events in Peru (XVI–XVIIIth Centuries): The Quinn *et al.* (1987) Chronology Revisited', in Ortlieb, L. and Macharé, J. (eds.), *Paleo-ENSO Records international symposium* (Extended abstracts), ORSTOM-CONCYTEC, Lima, Peru, pp. 143–149.

Kiladis, G. N. and Diaz, H. F.: 1989, 'Global Climatic Anomalies Associated with Extremes of the Southern Oscillation', *J. Clim.* **2**, 1069–1090.

Kuo, C., Lindberg, C., and Thomson, D. J.; 1990, 'Coherence Established between Atmospheric Carbon Dioxide and Global Temperature', *Nature* **343**, 709–714.

Manabe, S. and Stouffer, R. J.: 1988, 'Two Stable Equilibria of a Coupled Ocean-Atmosphere model', *J. Clim.* **1**, 841–866.

Michaelsen, J. and Thompson, L. G.: 1992, 'A Comparison of Proxy Records of El Niño/Southern Oscillation', in Diaz, H. F. and Markgraf, V. (eds.), *El Niño: Historical and Paleoclimatic Aspects of the Southern Oscillation*, Cambridge University Press, Cambridge, pp. 323–348.

Nicholls, N.: 1992, 'Historical El Niño/Southern Oscillation Variability in the Australasian Region', in Diaz, H. F. and Markgraf, V. (eds.), *El Niño: Historical and Paleoclimatic Aspects of the Southern Oscillation*, Cambridge University Press, Cambridge, pp. 151–173.

Park, J., Lindberg, C. R., and Vernon III, F. L.: 1987, 'Multitaper Spectral Analysis of High-Frequency Seismograms', *J. Geophys. Res.* **92**, 12,675–12,684.

Penland, C., Ghil, M., and Weickmann, K.: 1991, 'Adaptive Filtering and Maximum Entropy Spectra with Application to Changes in Atmospheric Angular Momentum', *J. Geophys. Res.* **96**, 22,659–22,671.

Quinn, W.H.: 1992, 'A Study of Southern Oscillation-Related Climatic Activity for A.D. 622–1990', in Diaz, H. F. and Markgraf, V. (eds.), *El Niño: Historical and Paleoclimatic Aspects of the Southern Oscillation*, Cambridge University Press, Cambridge, pp. 119–149.

Quinn, W. H., Neal, V. T., and Antunez de Mayolo, S. E.: 1987, 'El Niño over the Past Four and Half Centuries', *J. Geophys. Res.* **92**, 14449–14461.

Quinn, W. H. and Neal, W. T.: 1992, 'The Historical Record of El Niño Events', in Bradley, R. S. and Jones, P. D. (eds.), *Climate Since A.D. 1500*, Routledge, London, pp. 623–648.

Rasmusson, E. M., Wong, X. and Ropelewski, C. E.: 1990, 'The Biennial Component of ENSO Variability', *Journal of Marine Systems* **1**, 71–96.

Stocker, T. F. and Mysak, L. A.: 1992, 'Climatic Fluctuations on the Century Time Scale: A Review of High-Resolution Proxy Data and Possible Mechanisms', *Clim. Change* **20**, 227–250.

Thompson, L. G. and Mosley-Thompson, E.: 1989, 'One-Half Millennia of Tropical Climate Variability as Recorded in the Stratigraphy of the Quelccaya Ice Cap, Peru', in Peterson, D. H. (ed.), *Aspects of Climate Variability in the Pacific and the Western Americas*, Geophysical Monograph 55, Amer. Geo. Union, Washington, D.C., pp. 15–31.

Thomson, D. J.: 1982, 'Spectrum Estimation and Harmonic Analysis', *Proc. IEEE* **70**, 1055–1096.

Thomson, D. J.: 1990a, 'Time Series Analysis of Holocene Climate Data', *Phil. Trans. R. Soc. Lond.* **330**, 601–616.

Thomson, D. J.: 1990b, 'Quadratic-Inverse Spectrum Estimates: Applications to Paleoclimatology', *Phil. Trans. R. Soc. Lond.* **332**, 539–597.

Thomson, D. J. and Chave, A. D.: 1991, 'Jackknifed Error Estimates for Spectra, Coherences, and Transfer Functions', in Haykin, S. (ed.), *Advances in Spectrum Analysis and Array Processing*, Vol. I, pp. 58–113.

Trenberth, K. E. and Shea, D. J.: 1987, 'On the Evolution of the Southern Oscillation', *Mon. Wea. Rev.* **115**, 3078–3096.

Vautard, R. and Ghil, M.: 1989, 'Singular Spectrum Analysis in Nonlinear Dynamics with Applications to Paleoclimatic Time Series', *Physica D*, **35**, 395–424.

Vautard, R., Yiou, P., and Ghil, M.: 1992, 'Singular-Spectrum Analysis: A Toolkit for Short Noisy Chaotic Signals', *Physica D* **38**, 95–126.

Venrick, E. L., McGowan, J. A., Cayan, D. R., and Hayward, T. L.: 1987, 'Climate and Chlorophyll a: Long-Term Trends in the Central North Pacific Ocean', *Science* **238**, 70–72.

Villalba, R.: 1990, 'Climatic Fluctuations in Northern Patagonia during the Last 1000 Years as Inferred from Tree-Ring Records', *Quat. Res.* **34**, 346–360.

World Meteorological Organization: 1966, *Climatic Change*, WMO Tech. Note 79, 77 pp.

Wu, X. and Lough, J. M.: 1987, 'Estimating North Pacific Summer Sea Level Pressure back to 1600 Using Proxy Records from China and North America', *Adv. Atmos. Sci.* **4**, 74–84.

Ye, D., Fu, C., Chao, J., and Yoshino, M. (eds.): 1987, *The Climate of China and Global Climate*, Springer-Verlag, 441 pp.

Yiou, P., Genthon, C., Ghil, M., Jouzel, J., Le Treut, H., Barnola, J. M., Lorius, C., and Korotkevitch, Y. N.: 1991, 'High-Frequency Paleovariability in Climate and CO_2 Levels from Vostok Ice Core Records', *J. Geophys. Res.* **96**, 20, 365–20, 378.

Zhang, X., Song, J., and Zhao, Z.: 1989, 'The Southern Oscillation Reconstruction and Drought/Flood in China', *Acta Meteorol. Sinica.* **3**, 290–301.

(Received 19 January, 1993; in revised form 25 October, 1993).